Supporting Information

A Novel Orange-Red Thermally Activated Delayed Fluorescence Emitter with High Molecular Rigidity and Planarity Realizing 32.5% External Quantum Efficiency in Organic Light-Emitting Diodes

Heng-Yuan Zhang, [a] Hao-Yu Yang, [a] Ming Zhang, [a,b] Hui Lin, [a] Si-Lu Tao, [a] Cai-Jun Zheng,[*,a] and Xiao-Hong Zhang [b]

[a] School of Optoelectronic Science and Engineering, University of Electronic Science and Technology of China, Chengdu 610054, P. R. China.

E-mail: zhengcaijun@uestc.edu.cn

[b] Institute of Functional Nano & Soft Materials (FUNSOM), Soochow University, Suzhou 215123, P. R. China.

General Information

All reagents were purchased from commercial sources and used without further purification. Density functional theory (DFT) and time-dependent density functional theory (TD-DFT) simulations were performed using Gaussian 09 program package with the B3LYP/6-31g (d) basis set. Root-mean-square displacements (RMSDs) between S_0, S_1 and T_1 were calculated using VMD. The transition dipole moment (TDM) vector of $S_1 \rightarrow S_0$ was extracted from the TD-DFT results. The ^1H and ^{13}C NMR spectra were recorded in Dichloromethane-d2 and Chloroform-d, respectively via an Agilent DD2 400-MR spectrometer at room temperature. Mass spectra were obtained with a Shimadzu Biotech Axima Confidence high-resolution mass spectrometer. Thermogravimetric analysis (TGA) was performed on a TA Q600 system under a nitrogen atmosphere at a heating rate of 5 °C min^{-1}. Electrochemical analysis was carried out in N,N-Dimethylformamide (reductive scans) and Dichloromethane (oxidative scans) using tetrabutylammonium hexafluorophosphate as the supporting electrolyte with a CHI600E electrochemical analyzer. A platinum disk, a platinum wire

and an Ag electrode were respectively employed as the working, counter, and reference electrodes with standardized against ferrocenium/ferrocene (Fe^+/Fe). The UV-visible absorption spectra were measured with a Shimazu UV-2600 spectrophotometer and the photoluminescence spectra were recorded on a Hitachi F-4600 fluorescence spectrometer. Transient PL decay spectra were measured using Hamamatsu C11367-03 Quantaurus-Tau fluorescence lifetime measurement system. The excitation wavelength was 340 nm and the detection wavelength was 565 nm. Fluorescence quantum yields were measured using a Hamamatsu C11347 Quantaurus_QY absolute PL quantum yield spectrometer.

Synthesis of 11-bromodipyrido[3,2-a:2',3'-c]phenazine (1)

To a solution of 60 mL acetic acid, 4-bromobenzene-1,2-diamine (1.9 g, 10 mmol) and 1,10-phenanthroline-5,6-dione (2.3 g, 10 mmol) was added under nitrogen atmosphere. The mixture was stirred in a 250 mL round bottom flask at 120℃ for 24 h. After the reaction was complete, monitoring with TLC, ice water was added to the mixture and the generated precipitate was filtered under reduced pressure followed by recrystallization to obtain gray solid (3.2 g, yield 88.9%). ^{1}H NMR (400 MHz, Chloroform-d) δ 9.47 (td, J = 8.1, 1.7 Hz, 2H), 9.27 (d, J = 4.4 Hz, 2H), 8.44 (d, J = 2.1 Hz, 1H), 8.12 (d, J = 9.0 Hz, 1H), 7.93 (dd, J = 9.0, 2.1 Hz, 1H), 7.81 – 7.74 (m, 2H). MALDI-TOF-MS: m/z: calculated for $C_{18}H_9BrN_4$: 360.00, found: 360.86.

Synthesis of dipyrido[3,2-a:2',3'-c]phenazine (2NP)

The acceptor part was synthesized similar to intermediate 1 (416.5 mg, yield 73.8%). ^{1}H NMR (400 MHz, Chloroform-d) δ 9.66 (d, J = 8.1 Hz, 2H), 9.29 (s, 2H), 8.36 (s, 2H), 7.94 (s, 2H), 7.80 (s, 2H). MALDI-TOF-MS: m/z: calculated for $C_{18}H_{10}N_4$: 282.09, found: 282.96.

Synthesis of 10-(dipyrido[3,2-a:2',3'-c]phenazin-11-yl)-10H-spiro[acridine-9,9'-fluorene] (SAF-2NP)

A mixture of intermediate 1 (1.1 g, 3.0 mmol), 10H-spiro[acridine-9,9'-fluorene] (994.2

mg, 3 mmol), $Pd_2(dba)_3$ (275.0 mg, 0.3 mmol), DPEphos (162.0 mg, 0.3 mmol), and Cs_2CO_3 (3.9 g, 12.0 mmol) was added into a round bottom flask (100 mL) under nitrogen. 40 mL toluene was added to the reaction afterwards, and the mixture was refluxed for 24 h. After completion of the reaction, water and DCM was added to the cooled mixture. The organic layer was separated, and dried over Mg_2SO_4, and concentrated in vacuous. The residue solid was purified by column chromatography (ethyl acetate/dichloromethane, 1:3) and recrystallization to afford the product as orange solid (1.2 g, yield 65.4%). ^{1}H NMR (400 MHz, Methylene Chloride-d2) δ 9.72 (dd, J = 23.1, 8.1 Hz, 2H), 9.38 – 9.21 (m, 2H), 8.79 – 8.58 (m, 2H), 8.05 (dd, J = 8.8, 2.2 Hz, 1H), 7.99 – 7.76 (m, 4H), 7.52 (d, J = 7.5 Hz, 2H), 7.45 (t, J = 7.4 Hz, 2H), 7.35 (t, J = 7.4 Hz, 2H), 6.95 (t, J = 7.8 Hz, 2H), 6.63 (t, J = 7.5 Hz, 2H), 6.53 (d, J = 8.4 Hz, 2H), 6.45 (d, J = 7.9 Hz, 2H).; ^{13}C NMR (101 MHz, Chloroform-d) δ 156.25, 152.79, 152.75, 149.67, 148.09, 143.65, 143.11, 142.13, 141.73, 141.73, 141.42, 140.80, 139.27, 134.17, 132.80, 132.15, 128.44, 128.05, 127.73, 127.52, 127.34, 125.73, 125.27, 124.48, 121.24, 120.00, 114.66, 56.76. MALDI-TOF-MS: m/z: calculated for $C_{43}H_{25}N_5$: 611.21, found: 611.08.

Analysis of Rate Constants

Rate constants of SAF-2NP doped in 4,4'-N,N'-dicarbazolylbiphenyl (CBP) films with a 5% weight ratio were determined according to the following equations.[1]

$$k_d = \frac{1}{\tau_d} \quad \text{* MERGEFORMAT (1)}$$

$$k_p = \frac{1}{\tau_p} \quad \text{* MERGEFORMAT (2)}$$

$$k_{RISC} = \frac{k_p + k_d}{2} - \sqrt{\left(\frac{k_p + k_d}{2}\right)^2 - k_p k_d \left(1 + \frac{\Phi_d}{\Phi_p}\right)} \text{*}$$

MERGEFORMAT (3)

$$k_{ISC} = \frac{k_p k_d}{k_{RISC}} \frac{\Phi_d}{\Phi_p} \quad \text{* MERGEFORMAT (4)}$$

$$k_r = \frac{k_p k_d}{k_{RISC}} \Phi_{PL} \qquad \text{* MERGEFORMAT (5)}$$

$$k_{nr}{}^{S} = \frac{k_p k_d}{k_{RISC}} (1 - \Phi_{PL}) \qquad \text{* MERGEFORMAT (6)}$$

Where k_p and k_d are the decay rate constants for prompt and delayed fluorescence, respectively; τ_p and τ_d are the prompt fluorescence lifetime and delayed fluorescence lifetime, respectively; Φ_{PL}, Φ_p and Φ_d respectively represent the total, prompt and delayed fluorescence quantum efficiency; k_{RISC} is the rate constants of the RISC process; k_{ISC} represents the intersystem crossing rate; k_r is the rate constant of fluorescence decay; $k_{nr}{}^{S}$ represents non-radiative decay of singlet excitons.

Quantification of Emitting Dipole Moment

For the measurement of the orientation of emitting dipoles in molecules, a setup RSQX-01 made by the Changchun Ruoshui Technology Development Co., Ltd. was used. The samples were 30-nm-thick blend films of CBP:5 wt% SAF-2NP on fused silica substrates. The dipole orientation of the doped films was determined by angle-resolved and polarization-resolved PL on a half quartz cylinder prism. A continuous-wave He:Cd laser with a fixed angle of 45° to the substrate was employed as the excitation source. And *p*-Polarized emitted light was detected at the respective peak wavelength of the PL spectrum of each film.

Device Fabrication and Characterization

Indium tin oxide (ITO) glass substrates with a sheet resistance of 15 Ω per square were firstly cleaned with acetone, ethanol, and deionized water, and then dried in an oven at 120 °C for 2 h. Prior to being put into the thermal deposition instrument, the substrates were treated with UV-ozone for 20 minutes. All devices were fabricated by evaporating organic layers at a rate of 0.1-0.15 nm s^{-1} onto the ITO substrate sequentially at a pressure below 5×10^{-4} Pa. Onto the electron transporting layer, a layer of LiF with 1 nm thickness was deposited at a rate of 0.1 nm s^{-1} to improve electron injection. Finally, a 100-nm-thick layer of Al was deposited at a rate of 1 nm s^{-1} as the

cathode. The optical and electrical data of the devices were obtained with a PR655 Spectrscan and Keithley 2400 Source Meter under ambient atmosphere simultaneously. The current efficiencies (CEs), power efficiencies (PEs), and external quantum efficiencies (EQEs) were calculated with the data of current, luminance, and emission, assuming a Lambertian distribution.

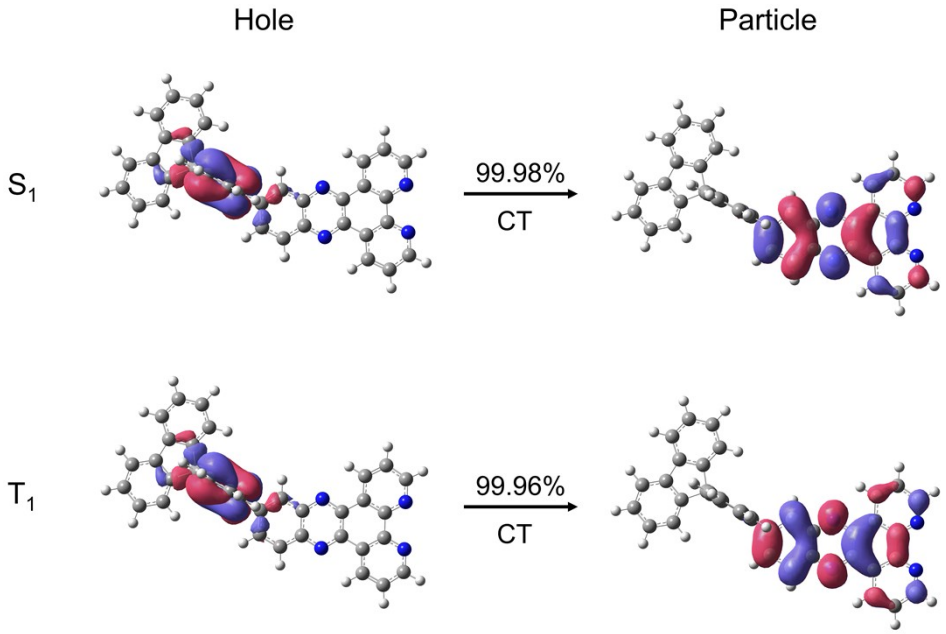

Figure S1. Natural transition orbitals (NTOs) of SAF-2NP.

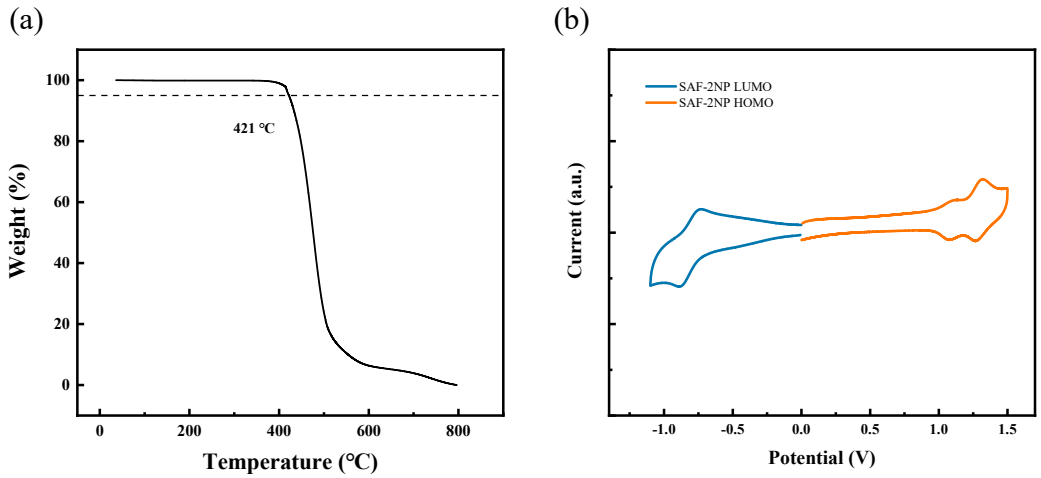

Figure S2. (a) Oxidation and reduction curves of SAF-2NP; (b) TGA traces of SAF-2NP recorded at a heating rate of 5℃ min^{-1}.

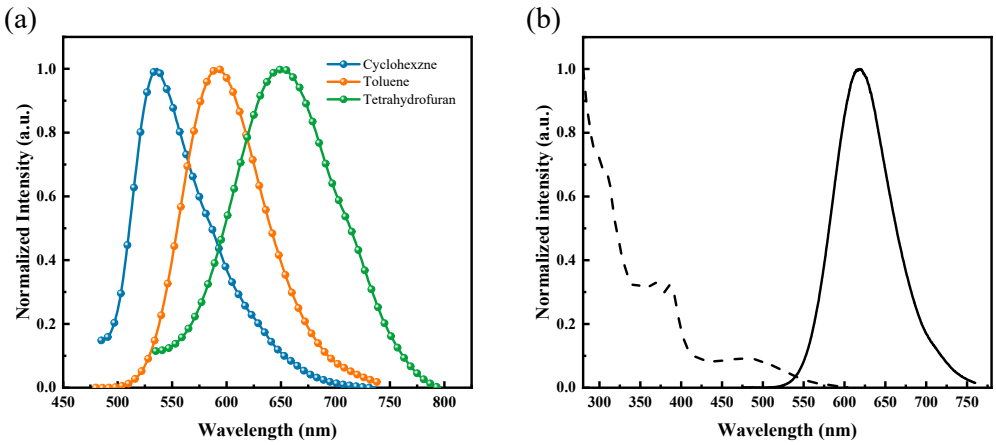

Figure S3. (a) Normalized fluorescence spectra of SAF-2NP in different solvents; (b) Normalized UV-vis and fluorescence spectra of the neat film of SAF-2NP.

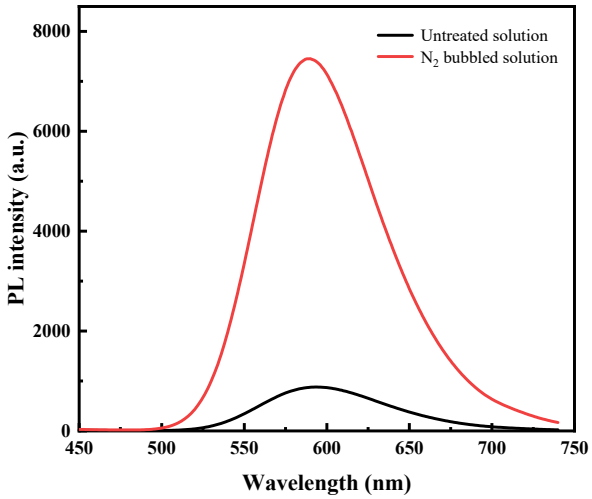

Figure S4. PL spectra of SAF-2NP in toluene solution before and after N2 bubbling.

Table S1. Photophysical parameters of SAF-2NP related to transient PL measurements, measured with CBP:5 wt% SAF-2NP films at 300K and calculated using Equation (1) to (6).

Compound	Φ_p/Φ_d [%]	τ_p [ns]	τ_d [μs]	A_1[a)]	A_2[a)]	k_r [10^7 s^{-1}]	k_{ISC} [10^7 s^{-1}]	k_{RISC} [10^5 s^{-1}]	k_{nr}^S [10^5 s^{-1}]
SAF-2NP	25/74	23	21	20123	66	1.07	3.25	1.91	1.08

[a)] Fitting parameters of the transient PL spectrum at 300K using the equation $y(t) = A_1 e^{-\frac{t}{\tau_p}} + A_2 e^{-\frac{t}{\tau_d}}$

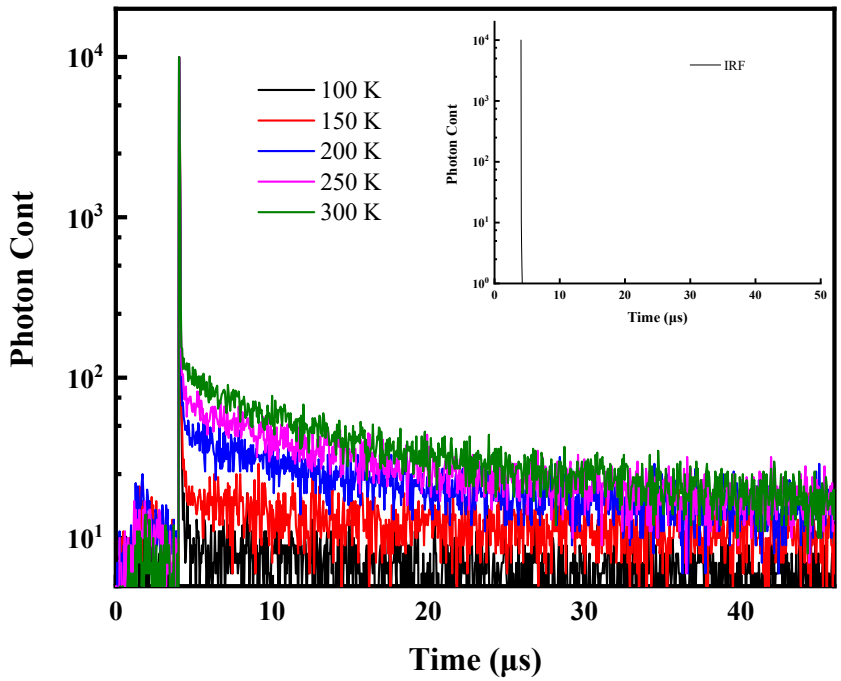

Figure S5. Temperature-dependent transient PL decay spectra measured with a CBP:5 wt% SAF-2NP film (Insert: IRF of the instrument).

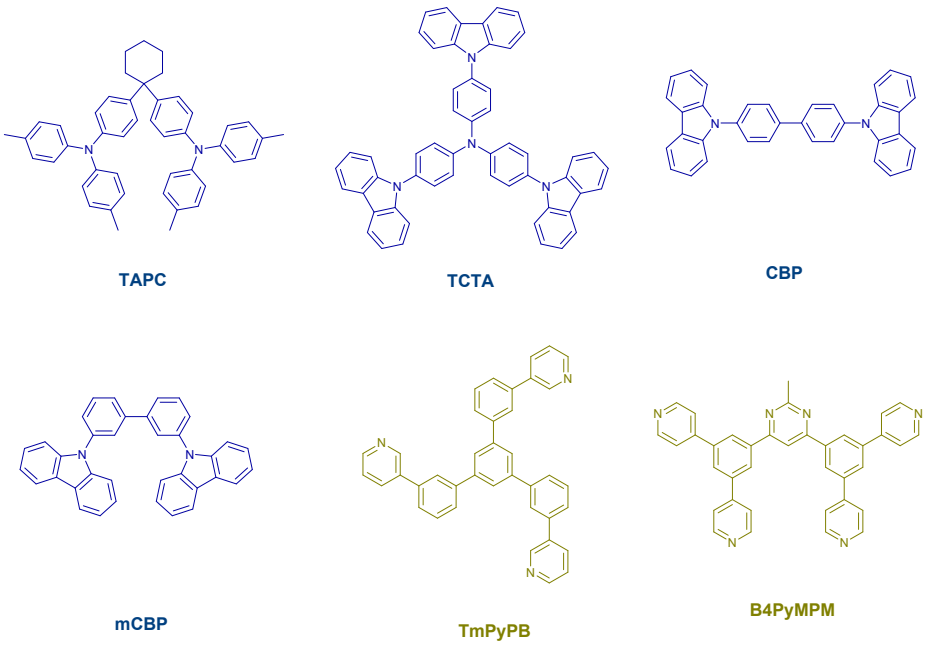

Figure S6 Materials used in SAF-2NP-based devices.

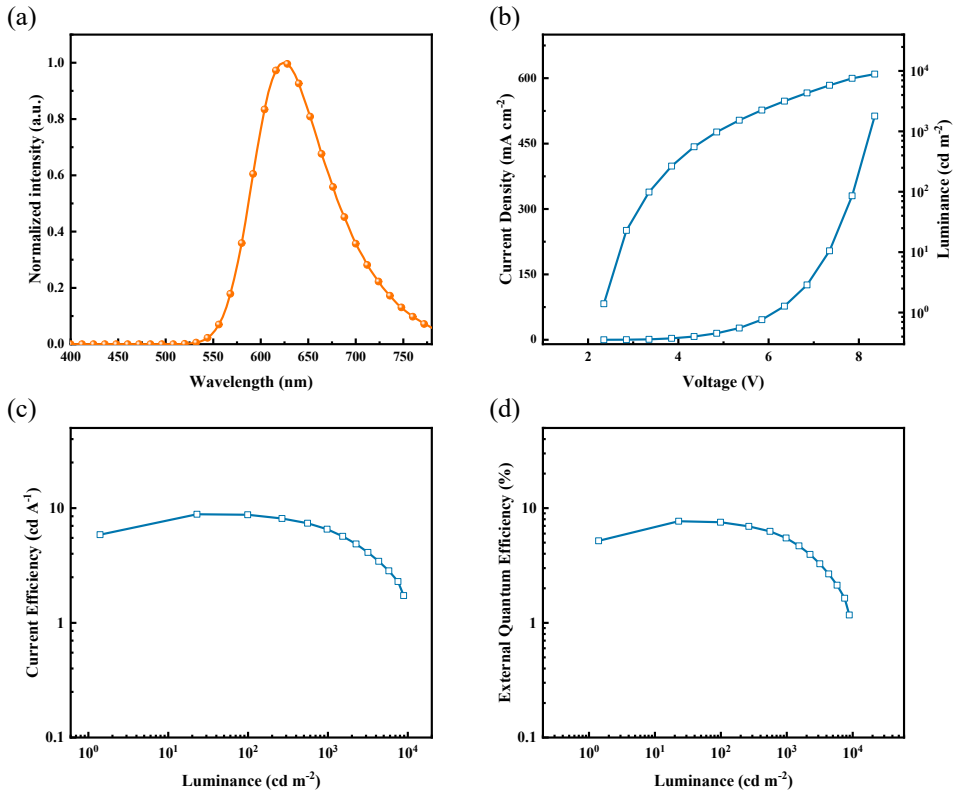

Figure S7. Performances of the non-doped OLED with a structure of indium tin oxide (ITO)/TAPC (35 nm)/TCTA (10 nm)/SAF-2NP (20 nm)/B4PyMPM (60 nm)/LiF (1 nm)/Al (100 nm). (a) The normalized electroluminescence spectrum; (b) The current density-voltage-luminance curve; (c) The current efficiency-luminescence curve; (d) The external quantum efficiency-luminescence curve.

Table S2. Summary of key performances of non-doped device.

V_{on}[a)] [V]	λ_{EL}[b)] [nm]	EQE_{max} [%]	CE_{max} [cd A^{-1}]	PE_{max} [lm W^{-1}]	CIE (x, y)[b)]	Performance at 100 and 1000 cd m^{-2}		
						EQE [%]	CE [cd A^{-1}]	PE [lm W^{-1}]
2.3	624	7.7	8.8	9.7	(0.64,0.37)	7.5/5.5	8.8/6.6	8.2/4.2

[a)] Turn-on voltage, voltage at brightness of 1 cd A-1. [b)] At 1,000 cd m^{-2}.

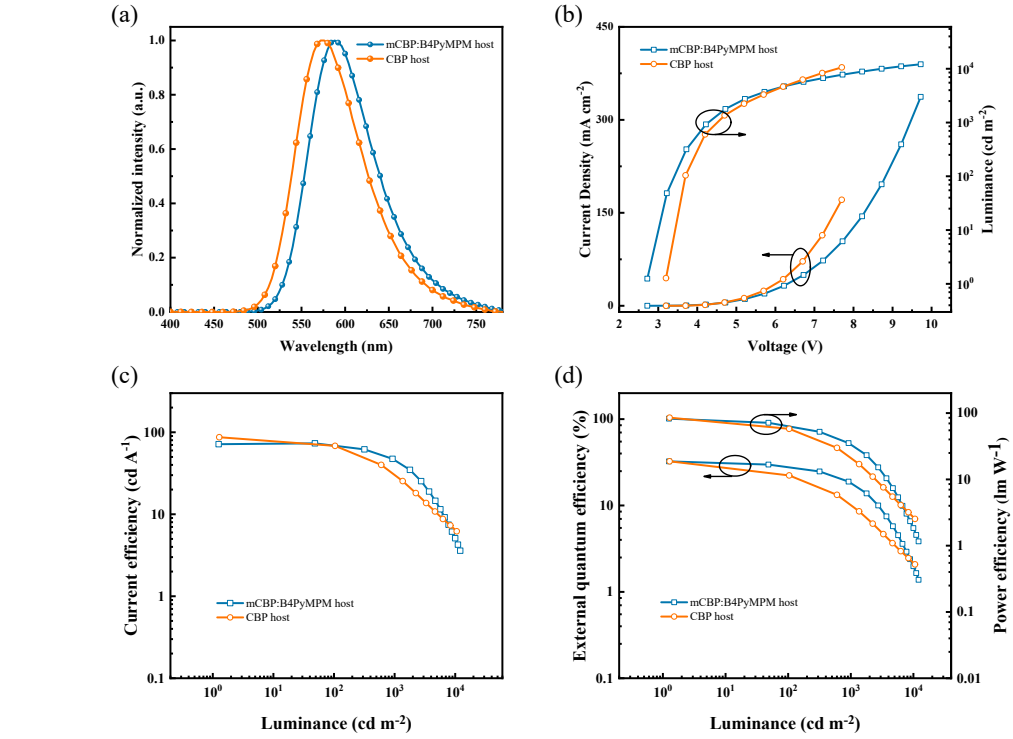

Figure S8. Performances of OLEDs using CBP and exciplex host. (a) The normalized electroluminescence spectrum; (b) The current density-voltage-luminance curve; (c) The current efficiency-luminescence curve; (d) The external quantum efficiency-luminescence curve.

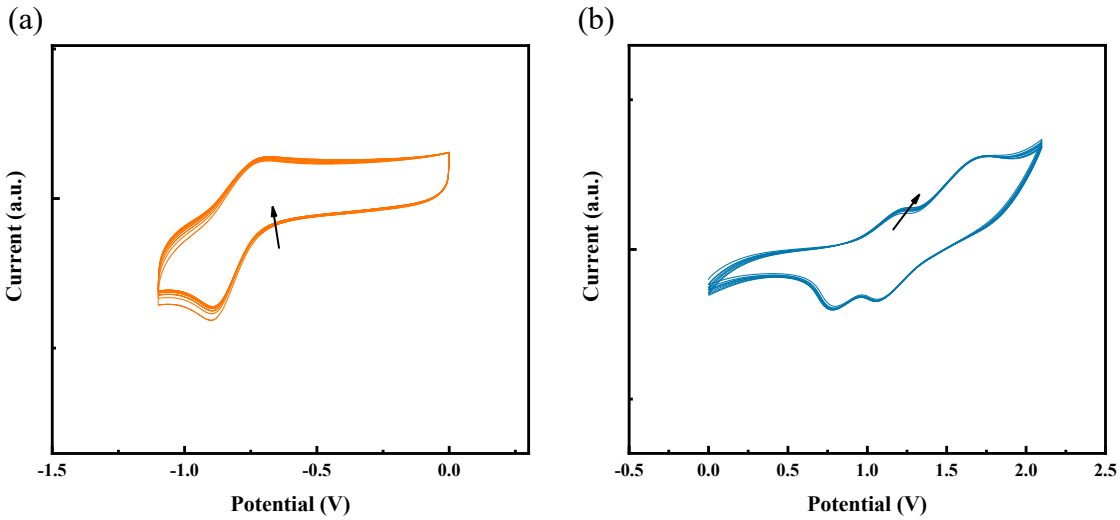

Figure S9. Multiple reductive (a) and oxidative (b) scans of SAF-2NP.

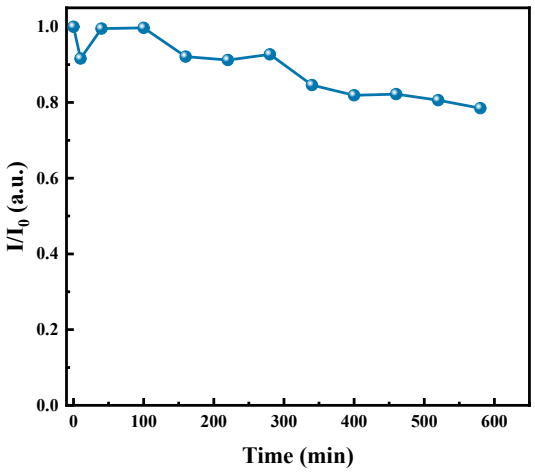

Figure S10. Photodegradation curves of the film (I_0: initial PL intensity of the pristine film; I: PL intensity after photodegradation).

To study the physicochemical stability of emitter, we conducted multiple scans in CV analysis and photostability measurement. Reductive and oxidative scans were carried out under the same conditions as described in the Supplementary Information. Both the reduction and oxidation curves remained nearly unchanged after multiple scans, suggesting good chemical stability. The photostability measurement was carried out in a glove box to exclude the effect of water and oxygen. The sample was a 60-nm thick film of SAF-2NP on glass substrate prepared through vacuum evaporation, which was excited at 5 cm away from a hand-hold UV light (Spectroline ENF-260C, 350 $\mu W/cm^2$ at 6 inches away). The pristine film demonstrated a peak intensity of 1147 and one of 900.1 was obtained after 580-min excitation, showing a mild decay of 21.5%. The photostability of SAF-2NP is superior than that of TBPe (decayed over 90% in less than 120 min) and FIrpic (decayed over 90% in about 300 min), and is comparable to that of some stable green TADF materials.[2]

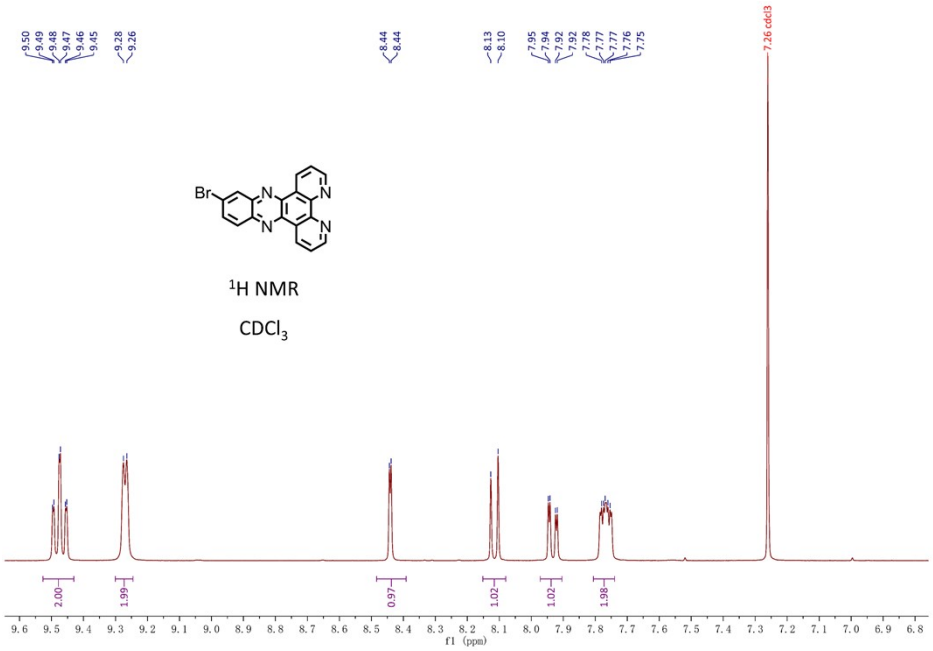

Figure S11. ^{1}H NMR spectra of intermediate 1.

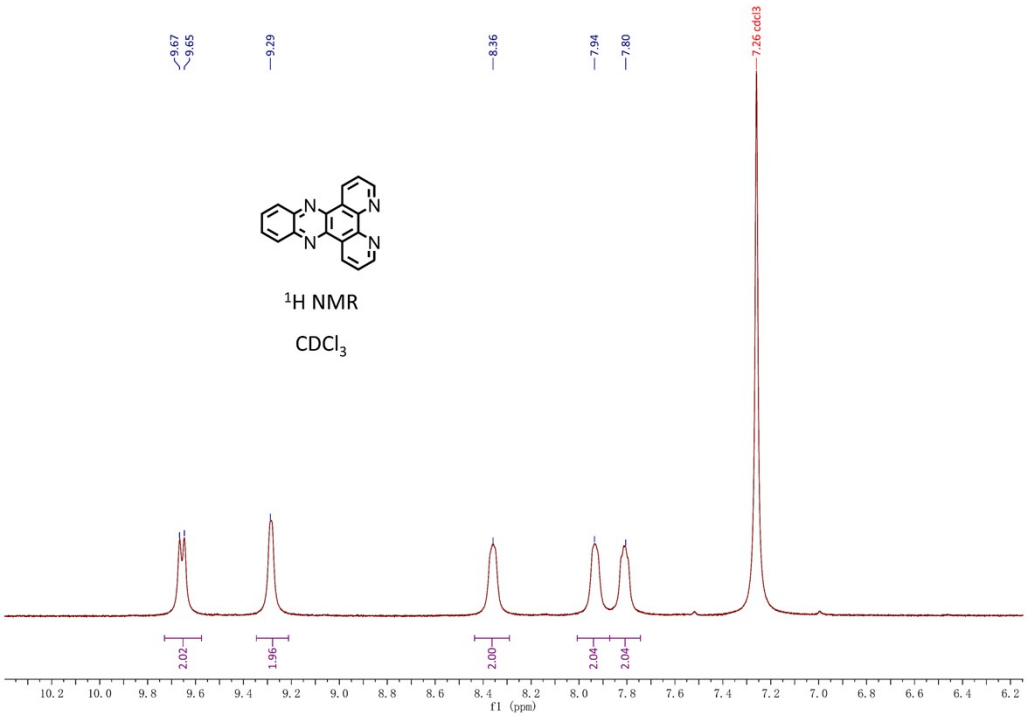

Figure S12. ^{1}H NMR spectra of 2NP.

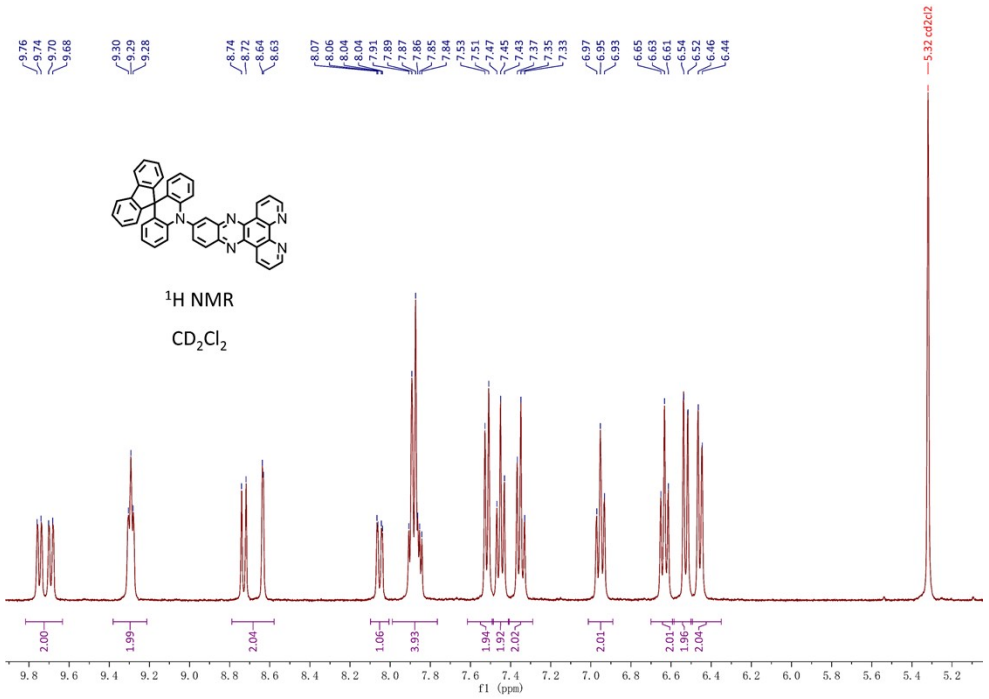

Figure S13. ^{1}H NMR spectra of SAF-2NP.

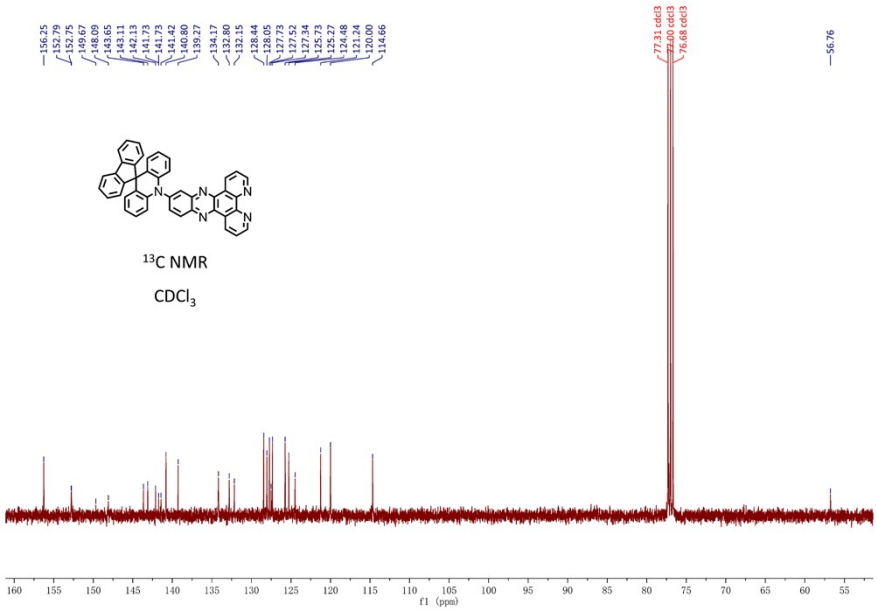

Figure S14. ^{13}C NMR spectra of SAF-2NP.

References

1. Y. Wada, H. Nakagawa, S. Matsumoto, Y. Wakisaka and H. Kaji, *Nature Photonics*, 2020, **14**, 643–649.

2. M. Yokoyama, K. Inada, Y. Tsuchiya, H. Nakanotani and C. Adachi, *Chem. Commun.*, 2018,**54**, 8261-8264